

# FROM PLANETESIMALS TO PLANETS IN TURBULENT PROTOPLANETARY DISKS I. ONSET OF RUNAWAY GROWTH

HIROSHI KOBAYASHI<sup>1</sup> HIDEKAZU TANAKA<sup>2</sup> AND SATOSHI OKUZUMI<sup>3</sup>

*Draft version December 23, 2015*

## ABSTRACT

When planetesimals grow via collisions in a turbulent disk, stirring through density fluctuation caused by turbulence effectively increases the relative velocities between planetesimals, which suppresses the onset of runaway growth. We investigate the onset of runaway growth in a turbulent disk through simulations that calculate the mass and velocity evolution of planetesimals. When planetesimals are small, the average relative velocity between planetesimals,  $v_r$ , is much greater than their surface escape velocity,  $v_{\text{esc}}$ , so that runaway growth does not occur. As planetesimals become large via collisional growth,  $v_r$  approaches  $v_{\text{esc}}$ . When  $v_r \approx 1.5v_{\text{esc}}$ , runaway growth of the planetesimals occurs. During the oligarchic growth subsequent to runaway growth, a small number of planetary embryos produced via runaway growth become massive through collisions with planetesimals with radii of that at the onset of runaway growth,  $r_{\text{p,run}}$ . We analytically derive  $r_{\text{p,run}}$  as a function of the turbulent strength. Growing  $\sim 10 M_{\oplus}$  embryos that are suitable to become the cores of Jupiter and Saturn requires  $r_{\text{p,run}} \sim 100$  km, which is similar to the proposed fossil feature in the size distribution of main belt asteroids. In contrast, the formation of Mars as quickly as suggested from Hf-W isotope studies requires small planetesimals at the onset of runaway growth. Thus, the conditions required to form Mars, Jupiter, and Saturn and the size distribution of the main-belt asteroids indicate that the turbulence increased in amplitude relative to the sound speed with increasing distance from the young Sun.

*Subject headings:* planets and satellites: formation — solar system: formation

## 1. INTRODUCTION

Planets are considered to be formed in a protoplanetary disk composed of gases and solids. In the standard scenario, kilometer-sized or larger planetesimals are generated from dust grains and collisional coagulation of the planetesimals forms planetary embryos. Once planetary embryos are as large as 10 Earth masses, the embryos start rapid gas accretion, which results in gas giant planets (Ikoma et al. 2000; Hori & Ikoma 2010; Mizuno 1980).

A swarm of planetesimals produces planetary embryos through runaway growth (Wetherill and Stewart 1989; Kokubo and Ida 1996; Ormel et al. 2010) and the embryos grow further through the accretion of remnant planetesimals, which is called oligarchic growth (Weidenschilling et al. 1997; Kokubo & Ida 1998). However, the stirring by embryos is so strong that collisions between planetesimals are destructive. The fragments produced by planetesimal collisions become progressively smaller by collisional cascade until 10 meter-sized fragments drift inward by gas drag (Kobayashi et al. 2010). The collisional fragmentation of planetesimals and the radial drift of small bodies that results from collisional fragmentation reduce the solid surface density of bodies surrounding planetary embryos, so that the growth of

the planetary embryos is stalled (Kobayashi et al. 2010, 2011). The collisional outcomes for kilometer-sized or larger planetesimals are determined by re-accretion of collisional fragments that result from shattering; therefore, the effective collisional strength is mainly controlled by self-gravity, so that larger planetesimals are collisionally stronger. Larger planetesimals can avoid a reduction of the solid surface density due to collisional fragmentation, which results in the formation of more massive planetary embryos. On the other hand, the timescale for planetary embryo formation through runaway and oligarchic growth is longer for larger planetesimals. Therefore, Kobayashi et al. (2011) found that the formation of 10 Earth mass cores inside 10 AU within 10 Myr requires moderate-sized planetesimals at the onset of runaway growth ( $\sim 100$  km in radius) in a massive disk ( $\sim 0.1$  solar masses).

Dust particles grow to meter-sized pebbles via collisions in a protoplanetary disk. Pebbles lose substantial angular momentum due to gas drag because of the sub-Keplerian rotational velocity of gas and spiral onto the central star. If pebbles are compact, then radial drift is too rapid to grow to planetesimals (Weidenschilling 1977). However, successive collisions of dust produce highly porous aggregates (Suyama et al. 2008, 2012). Icy porous aggregates that consist of a number of spherical sub-micron particles do not suffer from catastrophic disruption unless the impact velocities exceed 60–90 m/s (Wada et al. 2009, 2013). Okuzumi et al. (2012) investigated the collisional evolution of the mass and porosity of icy dust aggregates, whereby icy fluffy dust aggregates were determined to grow into planetesimals faster than they drift. The filling factor of the aggregates becomes as

hkobayas@nagoya-u.jp  
 hide@lowtem.hokudai.ac.jp  
 okuzumi@geo.titech.ac.jp

<sup>1</sup> Department of Physics, Nagoya University, Nagoya, Aichi 464-8602, Japan

<sup>2</sup> Institute of Low Temperature Science, Hokkaido University, Kita-Ku Kita 19 Nishi 8, Sapporo 060-0819, Japan

<sup>3</sup> Tokyo Institute of Technology, Ookayama, Meguro-ku, Tokyo 152-8551, Japan

low as  $\sim 10^{-5}$  when radial drift is most effective. Since the compaction of aggregates by ram pressure and self-gravity is effective with the growth of aggregates, the filling factor of kilometer-sized or larger planetesimals increases up to  $\sim 0.1$  (Kataoka et al. 2013a,b).

The critical collisional velocity that inhibits collisional growth is 80 m/s for icy dust aggregates (Wada et al. 2013). Such a high critical velocity means that icy planetesimals can be formed through collisions. Silicate dust aggregates may be destroyed at 8 m/s if the surface energy<sup>4</sup>  $\gamma$  of the particles is  $0.025 \text{ Jm}^{-2}$  (Wada et al. 2013). However, Kimura et al. (2015) pointed out that the surface energy of silicates depends on the outermost layer of absorbed water on the surfaces of dust particles. Thus, for a small amount of absorbed water,  $\gamma$  can be larger than  $0.1 \text{ Jm}^{-2}$  (Wiederhorn & Johnson 1971; Shchipalov 2000; Han et al. 2000; Roder et al. 2001; Tromans & Meech 2001). If  $\gamma = 0.25 \text{ Jm}^{-2}$ , then the critical collisional velocity of silicate aggregates can be larger than 50 m/s (Kimura et al. 2015), which allows the formation of silicate planetesimals via collisional growth. Therefore, here we consider planetesimal formation via the collisional coagulation of dust aggregates, while we ignore the alternative paths for planetesimal formation, such as streaming instability (Johansen et al. 2014).

The collisional growth of porous aggregates overcomes the drift barrier and the subsequent compaction of aggregates produces planetesimals with low porosity, which then grow further via collisions. Once gravitational focusing and dynamical friction are effective, the runaway growth of planetesimals occurs (Wetherill and Stewart 1989). Runaway growth produces a small number of planetary embryos, which then grow further via collisions with surrounding planetesimals that have radii similar to that at the onset of runaway growth. The lifetime of the surrounding planetesimals due to collisional fragmentation depends on their size (Kobayashi & Tanaka 2010; Kobayashi et al. 2010). Thus, the size of planetesimals at the onset of runaway growth affects the growth of planetary embryos.

Gravitational focusing and dynamical friction are effective if  $v_r \lesssim v_{\text{esc}}$ , where  $v_r$  is the relative velocity between planetesimals and  $v_{\text{esc}}$  is the mutual surface escape velocity of the planetesimals; however, runaway growth is suppressed if  $v_r \gtrsim v_{\text{esc}}$  (Wetherill and Stewart 1989). In protoplanetary disks, turbulent stirring due to hydrodynamical gas drag accelerates  $v_r$ , which is effective for bodies smaller than  $\sim 1 \text{ m}$ . On the other hand, the density fluctuation caused by turbulence results in significant perturbation that effectively increases the random velocities of kilometer-sized or larger planetesimals (Ida et al. 2008; Okuzumi & Ormel 2013; Ormel & Okuzumi 2013). Stirring by the density fluctuation in a turbulent disk suppresses the runaway growth of such kilometer-sized or larger planetesimals. Once runaway growth occurs, the planetary embryos formed are surrounded by a swarm of planetesimals with radii similar to that at the onset of runaway growth, which is similar to the condition resulting from previous studies starting from planetes-

imals (e.g., Kokubo and Ida 1996; Kokubo & Ida 1998; Inaba et al. 2001). Therefore, if representative planetesimals have radii of  $\sim 100 \text{ km}$  at the onset of runaway growth, as suggested in Kobayashi et al. (2011), then planetesimals may form massive cores to become gas giants.

Here, we investigate the collisional evolution of planetesimals by taking turbulent stirring into account. In Section 2, we introduce a model for turbulent stirring, collisional evolution, and protoplanetary disks. In Section 3, simulations are conducted for the collisional evolution of planetesimals in turbulent disks. In Section 4, the average relative velocities of planetesimals in a turbulent disk are analytically derived and the radius of the planetesimals at the onset of runaway growth is then determined. In Section 5, we discuss the radial profile of the turbulence strength required to form the Solar System. We summarize our conclusions in Section 6. In a separate paper (Paper II), continuous simulations are performed from the stage prior to runaway growth until the formation and growth of planetary embryos.

## 2. MODELING FOR COLLISIONAL GROWTH IN A TURBULENT DISK

### 2.1. Collisional Growth

Collisions between bodies at a distance  $a$  from the host star and the radial drift of bodies evolve the surface number density of bodies with masses ranging from  $m$  to  $m + dm$ ,  $n_s(m, a)dm$ , as

$$\begin{aligned} \frac{\partial m n_s(m, a)}{\partial t} = & \frac{m}{2} \int_0^\infty dm_1 \int_0^\infty dm_2 \\ & \times n_s(m_1, a) n_s(m_2, a) K(m_1, m_2) \\ & \times \delta(m - m_1 - m_2 + m_e) \\ & - m n_s(m) \int_0^\infty dm_2 n_s(m_2, a) K(m, m_2) \\ & + \frac{\partial}{\partial m} \int_0^\infty dm_1 \int_0^{m_1} dm_2 n_s(m_1, a) n_s(m_2, a) \\ & \times K(m_1, m_2) \Psi(m, m_1, m_2) \\ & - \frac{1}{a} \frac{\partial}{\partial a} [a m n_s(m, a) v_{\text{drift}}(m, a)], \end{aligned} \quad (1)$$

where  $m_e$  and  $\Psi(m, m_1, m_2)$  are, respectively, the total and cumulative masses of bodies ejected by a single collision between bodies with masses  $m_1$  and  $m_2$ ,  $v_{\text{drift}}$  is the drift velocity of a body due to gas drag, and

$$K(m_1, m_2) = (h_{m_1, m_2} a)^2 \langle \mathcal{P}_{\text{col}}(m_1, m_2) \rangle \Omega \quad (2)$$

where  $h_{m_1, m_2} = [(m_1 + m_2)/3M_*]^{1/3}$  is the reduced mutual Hill radius,  $\langle \mathcal{P}_{\text{col}}(m_1, m_2) \rangle$  is the dimensionless mean collisional rate, and  $\Omega$  is the Keplerian frequency. The collisional rate  $\langle \mathcal{P}_{\text{col}}(m_1, m_2) \rangle$  is given by a function of eccentricities and inclinations of colliding bodies, as summarized in Inaba et al. (2001).

The relative velocities between bodies are determined by their eccentricities and inclinations. The dispersions for eccentricities and inclinations change according to the gravitational interaction between bodies (Ohtsuki et al. 2002), damping by gas drag (Adachi et al. 1976), and collisional damping (Ohtsuki 1992). Stirring by turbulence is additionally taken into account and is introduced

<sup>4</sup> The adhesion energy between particles is proportional to  $\gamma^{5/3}$  (Johnson et al. 1971). The critical fragmentation velocity of aggregates composed of the particles is proportional to the square root of the adhesion energy (e.g.,  $\propto \gamma^{5/6}$ ) (Wada et al. 2009, 2013).

below. The eccentricity and inclination evolution is expressed as

$$\frac{de^2}{dt} = \left. \frac{de^2}{dt} \right|_{\text{grav}} + \left. \frac{de^2}{dt} \right|_{\text{drag}} + \left. \frac{de^2}{dt} \right|_{\text{coll}} + \left. \frac{de^2}{dt} \right|_{\text{turb}}, \quad (3)$$

$$\frac{di^2}{dt} = \left. \frac{di^2}{dt} \right|_{\text{grav}} + \left. \frac{di^2}{dt} \right|_{\text{drag}} + \left. \frac{di^2}{dt} \right|_{\text{coll}} + \left. \frac{di^2}{dt} \right|_{\text{turb}}, \quad (4)$$

where the subscripts “grav”, “drag”, “coll”, and “turb” indicate gravitational interaction, gas drag damping, collisional damping, and turbulent stirring, respectively. The damping rates by gas drag are given functions composed of the lowest order terms of  $e$  and  $i$  following Inaba et al. (2001) because  $e$  and  $i$  are much smaller than unity, although the damping rates by gas drag have higher order terms for high  $e$  and  $i$  as shown in Kobayashi (2015).

Turbulence stirring increases the random velocities of planetesimals, which delays the onset of runaway growth. Collisional destruction is less important before and during runaway growth in the disk without turbulence (Kobayashi et al. 2010). Therefore, collisional fragmentation is ignored by setting  $m_e = 0$  and  $\Psi(m, m_1, m_2) = 0$  in Eq. (1); however, this effect is investigated in Paper II.

For the initial condition, the respective surface densities of gas and solid are given by

$$\Sigma_g = 1.7 \times 10^3 x_g \left( \frac{a}{1 \text{ AU}} \right)^{-1.5} \text{ g cm}^{-2} \quad (5)$$

$$\Sigma_s = 30 f_{\text{ice}} x_s \left( \frac{a}{1 \text{ AU}} \right)^{-1.5} \text{ g cm}^{-2}, \quad (6)$$

where the ice factor  $f_{\text{ice}}$  is given as unity beyond the snow line,  $x_g$  and  $x_s$  are scaling factors, and the disk with  $x_g = x_s = 1$  corresponds to the minimum-mass solar nebula (MMSN) model (Hayashi 1981). We consider disks beyond the snow line ( $f_{\text{ice}} = 1$ ) around solar type stars with  $M_* = M_\odot$ . Disks ranging from 4.3 to 67 AU are treated using 8 radial meshes. Bodies initially have radii of 1 km and  $e = 10i = 6 \times 10^{-4}$ . As analytically shown in § 4, the results are almost independent of the initial size distribution,  $e$ , and  $i$  of the bodies. The solid surface density varies through collisional evolution and radial draft, whereas, for simplicity, the gas surface density does not change.

## 2.2. Turbulent Stirring

The turbulent stirring is given by

$$\left. \frac{de^2}{dt} \right|_{\text{turb}} = \left. \frac{de^2}{dt} \right|_{\text{std}} + \left. \frac{de^2}{dt} \right|_{\text{fs}}, \quad (7)$$

$$\left. \frac{di^2}{dt} \right|_{\text{turb}} = \left. \frac{di^2}{dt} \right|_{\text{std}} + \left. \frac{di^2}{dt} \right|_{\text{fs}}, \quad (8)$$

where the subscripts “std” and “fs” indicate density fluctuation stirring and frictional stirring, respectively. Each term is explained below.

Magnetorotational instability (MRI) induces turbulence in protoplanetary disks (e.g., Balbus & Hawley 1991; Suzuki et al. 2010). The excitation rate of eccentricities due to the density fluctuation caused by MRI

turbulence is given by (Okuzumi & Ormel 2013)

$$\left. \frac{de^2}{dt} \right|_{\text{sdf}} = f_d \left( \frac{\Sigma_g a^2}{M_*} \right)^2 \Omega \quad (9)$$

where  $f_d$  is the dimensionless factor dependent on the strength of the density fluctuation. Okuzumi & Ormel (2013) compiled previous results of magnetohydrodynamical simulations for MRI turbulent disks (Okuzumi & Hirose 2011; Gressel et al. 2012) and semi-analytically obtained  $f_d$ , given by

$$f_d = \frac{0.94 \mathcal{L} \alpha}{(1 + 4.5 H_{\text{res},0}/H)^2}, \quad (10)$$

where  $H$  is the scale height of the disk,  $H_{\text{res},0}$  is the half vertical width of the dead zone,  $\alpha$  is the dimensionless viscosity at the midplane of the disk scaled by the sound velocity and the scale height, and  $\mathcal{L}$  is a scale parameter of the order of unity. In this paper,  $\mathcal{L} = 1$  for simplicity.

Orbital inclination is also increased due to the density fluctuation. However, the excitation rate of inclination is much smaller than that of eccentricity in MRI turbulence. We assume

$$\left. \frac{di^2}{dt} \right|_{\text{sdf}} = \epsilon^2 \left. \frac{de^2}{dt} \right|_{\text{sdf}}, \quad (11)$$

where the coefficient  $\epsilon$  is much smaller than unity and of the order of 0.1 (Yang et al. 2012).  $\epsilon$  is set as 0.1.

The other turbulent stirring is caused by aerodynamical friction force (Völk et al. 1980). If the stopping time by gas drag is longer than the orbital period, then the stirring rates for random velocities are given by Youdin & Lithwick (2007) under the assumption of isotropic turbulence. The stirring rate of eccentricity is twice as large as that of inclination due to isotropic turbulence. Using the stirring rate given by Youdin & Lithwick (2007) under this assumption, the stirring rates are then approximated to be

$$\left. \frac{de^2}{dt} \right|_{\text{fs}} = \frac{4\alpha}{3\Omega t_{\text{stop}}^2} \left( \frac{c_s}{\Omega a} \right)^2, \quad (12)$$

$$\left. \frac{di^2}{dt} \right|_{\text{fs}} = \frac{2\alpha}{3\Omega t_{\text{stop}}^2} \left( \frac{c_s}{\Omega a} \right)^2, \quad (13)$$

where  $t_{\text{stop}}$  is the stopping time and  $t_{\text{stop}} \gg \Omega^{-1}$  is assumed. For a body with mass  $m$  and radius  $r_p$ ,

$$t_{\text{stop}} = \frac{2m}{\pi C_D r_p^2 \rho_{\text{gas}} u}, \quad (14)$$

where  $\rho_{\text{gas}}$  is the gas density,  $u$  is the relative velocity, and  $C_D$  is the dimensionless drag coefficient. Although  $C_D$  is given by a function of the Mach and Reynolds numbers in simulations according to Kobayashi et al. (2010),  $C_D \approx 0.5$  because bodies with  $r_p > 1$  km are treated in this paper.

Turbulent stirring via friction is important only for bodies  $\lesssim 100$  m. Although this stirring has little effect on the onset of runaway growth, it is included for consistency.

## 3. EVOLUTION OF SIZE DISTRIBUTION AND RANDOM VELOCITIES

Logarithmic mass bins are set with width  $\delta m = 1.05m$ , and the method developed by Kobayashi et al. (2010) is used to simultaneously integrate Eqs. (1), (3), and (4) to derive the time evolution of the size distribution, eccentricities, and inclinations. Fig. 1 shows  $m^2 n_s$  and  $e$  at 5.2 AU for  $x_s = x_g = 1$ ,  $f_d \approx 3.1 \times 10^{-4}$  ( $\alpha = 0.01$  and  $H_{\text{res},0} = H$ ), and the internal density of bodies of  $\rho_s = 1 \text{ g/cm}^3$ . The solid surface density is given by  $\Sigma_s \equiv \int m n_s dm = \int m^2 n_s d \ln m$ ; hence  $m^2 n_s$  indicates the surface density of planetesimals with masses around  $m$ . The planetesimal radius at the peak of  $m^2 n_s$  is given approximately by the weighted average radius of planetesimals, defined as

$$\bar{r}_p \equiv \frac{1}{\Sigma_s} \int r_p m n_s dm, \quad (15)$$

where  $r_p$  is the radius of a planetesimal with mass  $m$ . At the early stage ( $t \ll 2 \times 10^6 \text{ yr}$ ),  $m^2 n_s$  has a narrow peak around  $\bar{r}_p$ ; most planetesimals have radii similar to  $\bar{r}_p$ . This indicates the orderly growth of planetesimals. The shapes around the peak of  $m^2 n_s$  are similar over time. However, at  $\approx 2 \times 10^6 \text{ yr}$ , the runaway growth of planetesimals makes the peak wider (see Fig. 1). Note that the peak of the planetesimal size distribution is almost unchanged after runaway growth starts.

The eccentricities of planetesimals depend on the size of planetesimals (see Fig. 1). At  $r_p = \bar{r}_p$ ,  $e$  is approximately equal to  $e_{\text{col}}$  determined by the turbulent stirring, and the collisional growth and damping (see derivation in Section 4.1). For bodies larger than  $\bar{r}_p$ , the dynamical friction between bodies controls  $e$  if  $e < v_{\text{esc}}/v_K$ , where  $v_K = a\Omega$  is the Keplerian velocity. For bodies smaller than  $\bar{r}_p$ ,  $e$  is larger than  $e_{\text{col}}$  because collisional damping has little effect on  $e$  due to less frequent collisions between the bodies. The onset of runaway growth is determined by  $v_r \approx ev_K$  of planetesimals with  $\bar{r}_p$ . When  $\bar{r}_p$  is small,  $e$  for the planetesimals with  $\bar{r}_p$  is much larger than  $v_{\text{esc}}/v_K$ . Once  $e$  for the planetesimals with  $\bar{r}_p$  is close to  $v_{\text{esc}}/v_K$ , gravitational focusing is no longer negligible, which ignites the runaway growth of planetesimals. Runaway growth occurs at 40–60 km in radius. After the onset of runaway growth, the largest planetesimals grow faster than the planetesimals with weighted average radius. The stirring of the largest planetesimals that result from the runaway growth increases the eccentricities of planetesimals with  $\bar{r}_p$ .

Fig. 2 shows the evolution of  $\bar{r}_p$  and  $\bar{e}$  in the simulations (solid curves), where  $\bar{e}$  is the weighted average eccentricity, defined as

$$\bar{e} \equiv \frac{1}{\Sigma_s} \int e m n_s dm. \quad (16)$$

As  $\bar{r}_p$  increases,  $\bar{e}$  approaches  $v_{\text{esc}}/v_K$ . The runaway growth of planetesimals occurs at  $\bar{r}_p \approx 40\text{--}60 \text{ km}$  for  $f_d \approx 3.1 \times 10^{-4}$  and  $\rho_s = 1 \text{ g/cm}^3$  in the MMSN disk, as shown in Fig. 1. When  $\bar{r}_p$  becomes 40–60 km,  $\bar{e}$  is comparable to  $v_{\text{esc}}/v_K$  (see Fig. 2). For  $\bar{r}_p \gtrsim 90 \text{ km}$ ,  $\bar{e}$  rapidly increases with  $\bar{r}_p$ . The runaway growth of planetesimals rapidly produces planetesimals much larger than planetesimals with the weighted average radius. Fig. 1 also shows that stirring by the largest planetesimals produced by runaway growth increases the eccentricity of planetes-

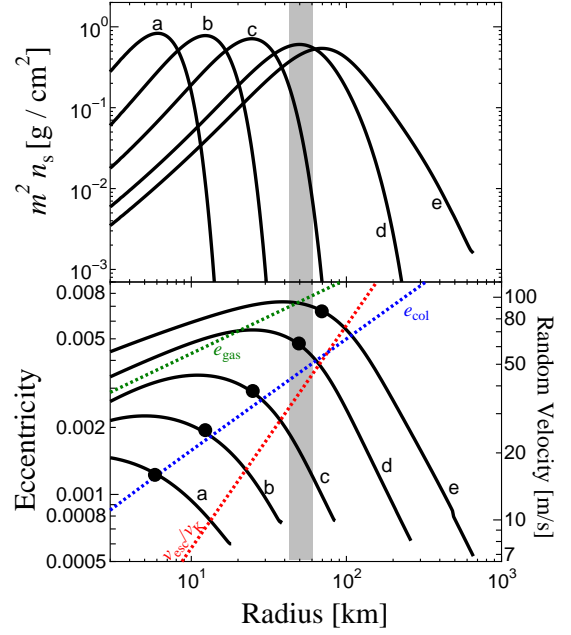


FIG. 1.— Surface density of planetesimals  $m^2 n_s$  (top), and eccentricity (bottom) at (a)  $1.3 \times 10^5 \text{ yr}$ , (b)  $3.6 \times 10^5 \text{ yr}$ , (c)  $8.9 \times 10^5 \text{ yr}$ , (d)  $2.3 \times 10^6 \text{ yr}$ , and (e)  $3.7 \times 10^6 \text{ yr}$  for  $x_g = x_s = 1$  (MMSN),  $\rho_s = 1 \text{ g/cm}^3$ ,  $\alpha = 10^{-2}$ , and  $H_{\text{res},0} = H$  ( $f_d \approx 3.1 \times 10^{-4}$ ) as a function of the radii of planetesimals. The runaway growth of planetesimals starts at the grey hatched area. Filled circles indicate eccentricities at the peak of  $m^2 n_s$ . The red, blue, and green dotted lines indicate  $v_{\text{esc}}/v_K$ ,  $e_{\text{col}}$  (Eq. 25), and  $e_{\text{gas}}$  (Eq. 28), respectively.

imals with  $\bar{r}_p$ .

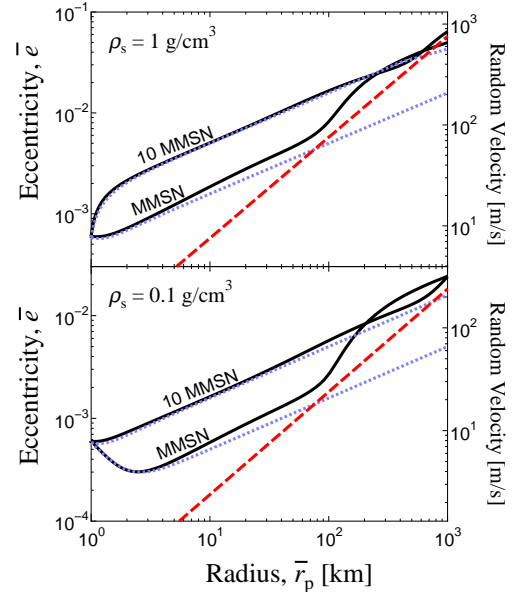


FIG. 2.— Relation between the weighted average radius and the weighted average eccentricity (black curves) during collisional growth for  $\rho_s = 1 \text{ g/cm}^3$  (top panel) and  $\rho_s = 0.1 \text{ g/cm}^3$  (bottom panel),  $r_{p0} = 1 \text{ km}$ ,  $f_d \approx 3 \times 10^{-4}$  ( $\alpha = 10^{-2}$  and  $H_{\text{res},0} = H$ ) at 5.2 AU in disks with  $x_g = x_s = 1$  (MMSN; bottom curves around 1 km) and 10 (10 MMSN; top curves around 1 km). Dotted curves (blue) indicate the smaller of  $e_{\text{col}}$  and  $e_{\text{gas}}$  given in Eqs. (25) and (28), respectively. Dashed lines (red) are the surface escape velocity divided by the Keplerian velocity for reference.

Fig. 3 shows the mass evolution of the largest planetesimals<sup>5</sup>,  $M$ , in the radial mesh around 5.2 AU. The mass evolution with time  $t$  is initially proportional to  $M \propto t^3$ . During orderly growth, gravitational focusing is less effective; namely,  $\dot{M}$  is proportional to  $M^{2/3}$ . Therefore, the time integration of  $\dot{M}$  results in  $M \propto t^3$ . However, the slopes  $d \ln M / d \ln t$  become steeper, which is explained by the stronger dependence of  $\dot{M}$  on  $M$  due to gravitational focusing. The increase of the slopes thus indicates the onset of runaway growth. Strong turbulence, i.e., large  $f_d$ , delays the onset of runaway growth. The onset of runaway growth increases  $d \ln M / d \ln t$  to greater than 3. The runaway radius, which is defined as the weighted average radius of planetesimals at  $d \ln M / d \ln t = 4$ , is obtained from the simulation in Fig. 4. The obtained runaway radius is in agreement with  $\bar{r}_p$  for  $\bar{e} \sim v_{\text{esc}}/v_K$  (see Figs. 1, 2, and 4). The runaway radius increases with  $f_d$ , so that the runaway growth is delayed due to strong turbulence.

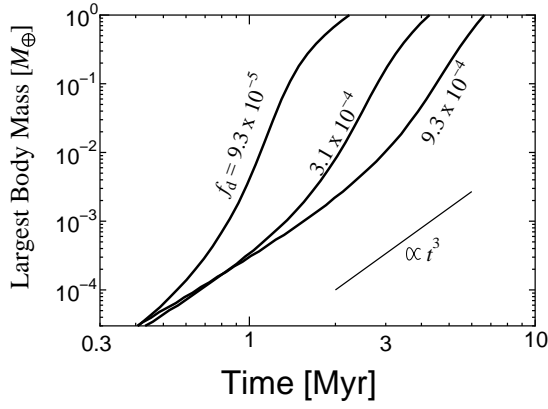


FIG. 3.— Time evolution of the mass of the largest planetesimals at 5.2 AU for  $\rho_s = 1 \text{ g/cm}^3$  and  $f_d \approx 9.3 \times 10^{-5}$ ,  $3.1 \times 10^{-4}$ , and  $9.3 \times 10^{-4}$ . The thin short line indicates the line proportional to  $t^3$  for reference.

For evolution from dust aggregates to pebble or planetesimal sized bodies, compaction due to the rearrangement of dust aggregates by self-gravity increases the filling factor of bodies and the internal density of bodies. However, the filling factor only increases up to  $\sim 0.1$  due to self-gravity (Kataoka et al. 2013b). According to the filling factor, the internal density of planetesimals is set to be  $\rho_s = 0.1 \text{ g/cm}^3$ . Fig. 5 shows the mass and velocity evolution of planetesimals for  $\rho_s = 0.1 \text{ g/cm}^3$  in the MMSN disk with  $f_d \approx 3.1 \times 10^{-4}$ . The random velocity is smaller than that for high  $\rho_s$  because collisional damping and gas drag are more effective. However,  $v_{\text{esc}}$  is smaller for lower  $\rho_s$ , so that runaway growth of the bodies occurs at 40–50 km in radius, which is similar to the result for  $\rho_s = 1 \text{ g/cm}^3$ . Interestingly, the radius at the onset of the runaway growth of bodies is almost independent of  $\rho_s$  (see also Fig. 4).

#### 4. ANALYTIC SOLUTION FOR ORDERLY GROWTH IN A TURBULENT DISK

<sup>5</sup> The mass of the largest bodies is given by the average mass of “runaway bodies” defined in Kobayashi et al. (2010).

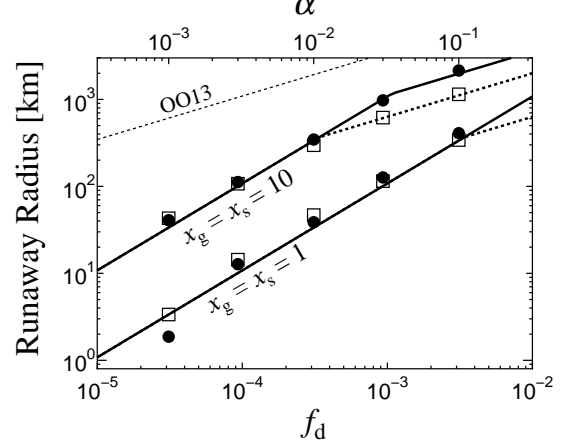


FIG. 4.— Weighted average radius of planetesimals at the onset of runaway growth obtained from simulations for  $\rho_s = 1 \text{ g/cm}^3$  (open squares) and  $0.1 \text{ g/cm}^3$  (filled circles), as a function of  $f_d$  or  $\alpha$  for  $H_{\text{res},0} = H$ . The lines correspond to the smaller of  $r_{p,\text{run},c}$  and  $r_{p,\text{run},g}$  given by Eqs. (29) and (30) with  $\xi_1 = \xi_2 = 1.5$ , respectively, for  $\rho_s = 1 \text{ g/cm}^3$  (dotted) and  $0.1 \text{ g/cm}^3$  (solid). The thin dotted line indicates the analytical estimate of the runaway radius by Ormel & Okuzumi (2013) for  $\rho_s = 1 \text{ g/cm}^3$  in 10 MMSN.

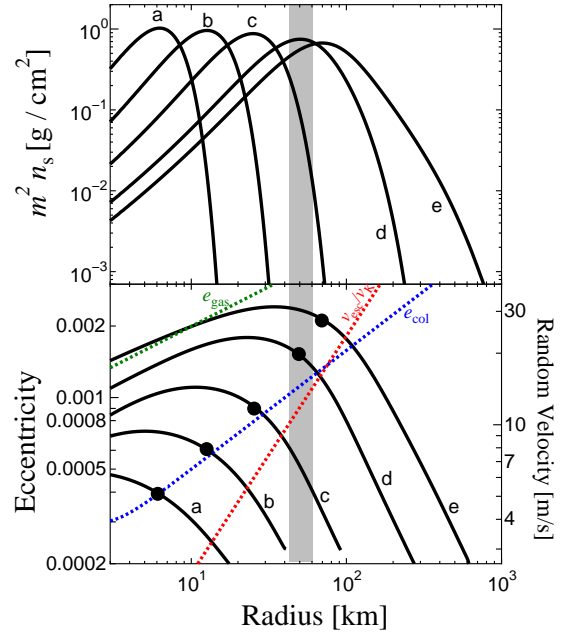


FIG. 5.— Same as Fig. 1, but for  $\rho_s = 0.1 \text{ g/cm}^3$  at (a)  $1.4 \times 10^4$  yr, (b)  $3.6 \times 10^4$  yr, (c)  $8.9 \times 10^4$  yr, (d)  $2.3 \times 10^5$  yr, and (e)  $3.6 \times 10^5$  yr.

The mass distribution of planetesimals depends on the mass growth rate,  $\dot{m}$ . If  $p \equiv d \ln \dot{m} / d \ln m < 1$ , smaller bodies grow faster and the orderly growth of bodies then occurs; bodies with the weighted average radius, which approximately determines the solid surface density, is comparable to the radius of the largest bodies. The collisional evolution of dust aggregates is an example of orderly growth (e.g., Okuzumi et al. 2012). However, if  $p \geq 1$ , then larger bodies grow faster and hence the runaway growth of bodies occurs; the weighted average radius becomes much smaller than the radius of the largest

bodies.

The growth rate  $\dot{m}$  is proportional to the collisional cross section between bodies with radii  $r_1$  and  $r_2$ , given by  $\pi(r_1 + r_2)^2(1 + \Theta)$ , where  $\Theta = v_{\text{esc}}^2/v_r^2$  is the Safronov parameter. When  $v_r$  is much smaller than  $v_{\text{esc}}$  ( $\Theta \gg 1$ ),  $\dot{m} \propto m^{4/3}v_r^{-2}$ . The collisional growth phase of bodies is determined by the mass dependence of  $v_r$ . The cross section of gravitational interaction is proportional to the 90 degree scattering cross section given by  $\pi(r_1 + r_2)^2\Theta^2$ , which is larger than the collisional cross section for  $\Theta \gtrsim 1$ . The dynamical friction caused by gravitational interaction results in the energy equipartition of bodies. If bodies mainly grow through collisions with similar sized bodies, then the random velocities of bodies are proportional to  $m^{-1/2}$  due to equipartition, which results in  $\dot{m} \propto m^{7/3}$ .  $p$  is then larger than unity and runaway growth occurs. Therefore,  $\Theta$  is very important to derive the radius of planetesimals at the onset of runaway growth, and hence, we first derive the random velocity of planetesimals in a turbulent disk.

The random velocity of planetesimals stirred by the density fluctuation caused by turbulence can exceed the surface escape velocity of the planetesimals ( $\Theta < 1$ ). Gravitational focusing and dynamical friction are suppressed for  $\Theta < 1$ ; therefore, orderly growth occurs until the relative velocity is comparable to the escape velocity. During orderly growth, a monodisperse population of planetesimals with mass  $m$  and radius  $r_p$  can be assumed in each narrow annulus of the disk. Ormel & Okuzumi (2013) analytically derived the random velocity through the equilibrium between stirring by turbulence and damping by gas drag and the radius of planetesimals at the onset of runaway growth, using the equilibrium velocity. However, collisional damping and growth are also important to determine the random velocity. The runaway radii obtained by simulations are thus much smaller than their estimates (Fig. 4). In this section, we derive the random velocity from turbulent stirring with the effect of collisions or with the damping by gas drag to derive the radius of planetesimals at the onset of runaway growth.

#### 4.1. Random Velocity

Damping by mutual collisions decreases eccentricity. The eccentricity  $e_{12}$  of the body at the barycenter of colliding planetesimals with masses  $m_1$ ,  $m_2$  and eccentricities  $e_1$ ,  $e_2$  is given by (Ohtsuki 1992)

$$e_{12}^2 = \left(\frac{m_1}{m_1 + m_2}\right)^2 e_1^2 + \left(\frac{m_2}{m_1 + m_2}\right)^2 e_2^2, \quad (17)$$

which is derived under the assumption of the random distribution of the longitudes of perihelion and the ascending nodes. Collisions between planetesimals with similar masses are dominant prior to runaway growth; therefore, a single merging collision decreases the square of eccentricity by a factor of 1/2.

The surface number density of planetesimals is  $\Sigma_s/m$ , the collisional cross section is approximated to  $\pi r_p^2$  because  $v_r \gg v_{\text{esc}}$ , the relative velocity is approximated as  $ea\Omega$  because  $e \gg i$ , and the “scale height” of planetesimals is given by  $ia$ ; therefore, the collisional rate is approximately given by  $(\Sigma_s/m)\pi r_p^2(e/i)\Omega$ . A more ac-

curate collisional rate between planetesimals is given by  $(\Sigma_s/m)h_{m,m}^2 a^2 \langle \mathcal{P}_{\text{col}}(m, m) \rangle \Omega$  (cf. Eq. 1). If  $ev_K \gg v_{\text{esc}}$  and  $e \gg i$ , then  $h_{m,m}^2 a^2 \langle \mathcal{P}_{\text{col}}(m, m) \rangle \approx C_{\text{col}} r_p^2 e/i$ , where  $C_{\text{col}} = 4.8$  (Inaba et al. 2001). The error of the crude estimate for the collisional rate is a factor  $C_{\text{col}}/\pi \approx 1.5$ . The collisional rate multiplied by  $-e^2/2$  is equal to  $de^2/dt$ ; therefore, the collisional damping rate for bodies with mass  $m$  and radius  $r_p$  is given by

$$\left. \frac{de^2}{dt} \right|_{\text{coll}} = -C_{\text{col}} \frac{e^3}{2i} \frac{r_p^2 \Sigma_s}{m} \Omega. \quad (18)$$

The collisional damping for inclination is obtained in the same way, as

$$\left. \frac{di^2}{dt} \right|_{\text{coll}} = -C_{\text{col}} \frac{ie}{2} \frac{\Sigma_s r_p^2}{m} \Omega. \quad (19)$$

From Eqs. (9), (11), (18), and (19), the time derivatives of  $e^2$  and  $i^2$  are given by

$$\frac{de^2}{dt} = f_d \left( \frac{\Sigma_g a^2}{M_*} \right)^2 \Omega - C_{\text{col}} \frac{e^3}{2i} \frac{r_p^2 \Sigma_s}{m} \Omega, \quad (20)$$

$$\frac{di^2}{dt} = \epsilon^2 f_d \left( \frac{\Sigma_g a^2}{M_*} \right)^2 \Omega - C_{\text{col}} \frac{ie}{2} \frac{r_p^2 \Sigma_s}{m} \Omega. \quad (21)$$

From Eqs. (20) and (21),

$$\frac{d}{dt} \left( \frac{i}{e} \right) = \left( \epsilon^2 - \frac{i^2}{e^2} \right) \frac{f_d}{2ei} \left( \frac{\Sigma_g a^2}{M_*} \right)^2 \Omega. \quad (22)$$

Interestingly, the time derivative of  $i/e$  is independent of collisional damping but depends only on the stirring. In the steady state for  $i/e$ , Eq. (22) gives  $i/e = \epsilon$ .

The equilibrium eccentricity obtained from  $de^2/dt = 0$  in Eq. (20) is overestimated (cf. Ida et al. 2008) because the timescale of collisional damping is comparable to that of collisional growth. Therefore, the effect of collisional growth should be taken into account. The collisional growth rate of bodies is given by

$$4\pi r_p^2 \rho_s \frac{dr_p}{dt} = \frac{C_{\text{col}}}{\epsilon} r_p^2 \Sigma_s \Omega, \quad (23)$$

where  $i/e = \epsilon$  is applied. From Eqs. (20) and (23),  $de^2/dr_p$  is obtained as

$$\frac{de^2}{dr_p} = \frac{4\pi f_d \epsilon}{C_{\text{col}}} \left( \frac{\Sigma_g a^2}{M_*} \right)^2 \left( \frac{\rho_s}{\Sigma_s} \right) - \frac{3e^2}{2r_p}. \quad (24)$$

From the integration of Eq. (24) over  $r_p$ , the collision-turbulence dominated eccentricity,  $e_{\text{col}}$ , is given by

$$e_{\text{col}}^2 = \frac{8\pi \epsilon f_d \rho_s r_p}{5C_{\text{col}} \Sigma_s} \left( \frac{\Sigma_g a^2}{M_*} \right)^2 \left[ 1 - \left( \frac{r_p}{r_{p0}} \right)^{-5/2} \right] + e_0^2 \left( \frac{r_p}{r_{p0}} \right)^{-3/2}, \quad (25)$$

where  $r_{p0}$  and  $e_0$  are the initial radius and eccentricity, respectively. If  $r_p \gg r_{p0}$ , then

$$e_{\text{col}} \approx \left( \frac{8\pi f_d \epsilon \rho_s r_p}{5C_{\text{col}} \Sigma_s} \right)^{1/2} \left( \frac{\Sigma_g a^2}{M_*} \right)$$

$$\approx 1.5 \times 10^{-4} \left( \frac{f_d}{10^{-4}} \right)^{1/2} \left( \frac{r_p}{1 \text{ km}} \right)^{1/2} \left( \frac{\Sigma_g}{140 \text{ g cm}^{-2}} \right) \times \left( \frac{\Sigma_s}{2.5 \text{ g cm}^{-2}} \right)^{-1/2} \left( \frac{\rho_s}{0.1 \text{ g cm}^{-3}} \right)^{1/2}. \quad (26)$$

The equilibrium eccentricity easily estimated from  $de^2/dt = 0$  in Eq. (20) with  $i/e = \epsilon$  is overestimated by a factor of  $\sqrt{5/3}$ .

On the other hand, for large planetesimals and/or small  $\Sigma_s$ , the eccentricity damping by gas drag is more effective than the collisional effects. The turbulent stirring given by Eq. (9) increases  $e$  effectively, so that  $v_r = ev_K$  is much greater than  $iv_K$  and the velocity difference between  $v_K$  and the rotational velocity of gas. The stopping timescale by gas drag is  $\sim (m/\pi r_p^2)(H/\Sigma_g)(1/ea\Omega)$  (Adachi et al. 1976). The  $e^2$ -damping rate via gas drag is approximately given by  $e^2$  divided by the stopping time. The  $e^2$ -damping rate is given by

$$\left. \frac{de^2}{dt} \right|_{\text{gas}} = -B \frac{\Sigma_g}{\rho_s r_p} \frac{a}{H} e^3 \Omega, \quad (27)$$

where  $B \simeq 0.378$  is the correction factor obtained from accurate treatment of  $e$ -damping and orbital averaging (Adachi et al. 1976). The equilibrium eccentricity between gas damping and turbulent stirring is obtained from Eqs. (9) and (27), given by

$$e_{\text{gas}} = \left( \frac{f_d \rho_s r_p \Sigma_g a^3 H}{B M_*^2} \right)^{1/3} \approx 6.3 \times 10^{-4} \left( \frac{f_d}{10^{-4}} \right)^{1/3} \left( \frac{r_p}{1 \text{ km}} \right)^{1/3} \left( \frac{\Sigma_g}{140 \text{ g cm}^{-2}} \right)^{1/3} \times \left( \frac{a}{5.2 \text{ AU}} \right)^{4/3} \left( \frac{H}{0.071 a} \right)^{1/3} \left( \frac{\rho_s}{0.1 \text{ g cm}^{-3}} \right)^{1/3}. \quad (28)$$

If  $r_p \gtrsim 6000 \text{ km}$  (600 km) for  $\rho_s = 0.1 \text{ g cm}^{-3}$  ( $1 \text{ g cm}^{-3}$ ) in the MMSN disk with  $f_d = 10^{-4}$ , then  $e_{\text{gas}} \lesssim e_{\text{col}}$ . The damping by gas drag is thus less effective than collisions unless planetesimals are very large.

The smaller of analytic solutions,  $e_{\text{col}}$  and  $e_{\text{gas}}$ , reproduces the evolution curves given by simulations unless the runaway growth of planetesimals begins (see Fig. 2). After the runaway growth,  $e$  of the representative planetesimals is mainly controlled by stirring due to the largest planetesimals, so that the analytic solutions are no longer valid.

#### 4.2. Runaway Radius

Once  $ev_K \sim v_{\text{esc}}$ , runaway growth starts due to gravitational focusing and dynamical friction. For  $e \approx e_{\text{col}}$ , the radius of planetesimals at the onset of runaway growth,  $r_{p,\text{run,c}}$ , is determined by  $e_{\text{col}} = \xi_1 v_{\text{esc}}/v_K$  with  $\xi_1 \sim 1$ . Using Eq. (25),  $r_{p,\text{run,c}}$  is given by

$$r_{p,\text{run,c}} = \frac{3\epsilon f_d \Sigma_g^2 a^3}{5\xi_1^2 C_{\text{col}} \Sigma_s M_*}, \approx 100 \left( \frac{\xi_1}{1.5} \right)^{-2} \left( \frac{f_d}{10^{-3}} \right) \left( \frac{a}{5.2 \text{ AU}} \right)^3 \left( \frac{\Sigma_s}{2.5 \text{ g cm}^{-2}} \right)^{-1}$$

$$\times \left( \frac{\Sigma_g}{140 \text{ g cm}^{-2}} \right)^2 \left( \frac{M_*}{M_\odot} \right)^{-1} \text{ km}, \quad (29)$$

where  $r_{p,\text{run,c}} \gg r_{p0}$  is assumed. Interestingly  $r_{p,\text{run,c}}$  is independent of  $\rho_s$ , which is in agreement with the simulation results (see Fig. 4).

If  $e$  is determined by  $e_{\text{gas}}$ , then the radius of planetesimals at the onset of runaway growth,  $r_{p,\text{run,g}}$ , is obtained from  $e_{\text{gas}} = \xi_2 v_{\text{esc}}/v_K$  as

$$r_{p,\text{run,g}} = \xi_2^{-3/2} \left( \frac{27 f_d^2 \Sigma_g^2 H^2 a^3}{512 \pi^3 B^2 \rho_s M_*} \right)^{1/4} \approx 350 \left( \frac{\xi_2}{1.5} \right)^{-3/2} \left( \frac{f_d}{10^{-3}} \right)^{1/2} \left( \frac{H}{0.071 a} \right)^{1/2} \times \left( \frac{a}{5.2 \text{ AU}} \right)^{3/4} \left( \frac{\Sigma_g}{140 \text{ g cm}^{-2}} \right)^{1/2} \times \left( \frac{\rho_s}{0.1 \text{ g cm}^{-3}} \right)^{-1/4} \left( \frac{M_*}{M_\odot} \right)^{-1/4} \text{ km}. \quad (30)$$

Ormel & Okuzumi (2013) derived a formula similar to Eq. (30) from the equilibrium between the turbulence stirring and gas drag damping. The formula derived by Ormel & Okuzumi (2013) overestimates by a factor of approximately 3.1 when compared to Eq. (30) with the realistic value of  $\xi_2 = 1.5$  (see also Fig. 4).

The runaway radii given by simulations are consistent with those obtained from the analytic formulae. Assuming  $\xi_1 = \xi_2 = 1.5$ , the smaller of  $r_{p,\text{run,c}}$  and  $r_{p,\text{run,g}}$  reproduces the radius of planetesimals at the onset of runaway growth,  $r_{p,\text{run}}$ , obtained from the simulations (see Fig. 4). The runaway radius is determined by  $r_{p,\text{run,c}}$  for small  $f_d$ , while  $r_{p,\text{run}} \approx r_{p,\text{run,g}}$  for large  $f_d$ . Strong turbulence (high  $f_d$ ) causes  $r_{p,\text{run}}$  to be large. This dependence is explained by Eqs. (29) and (30). If  $r_{p,\text{run}} \lesssim 300 \text{ km}$  around 5 AU, then  $r_{p,\text{run}}$  is determined by  $r_{p,\text{run,c}}$ ; therefore, the effects of collisions are more important to determine the runaway radius.

#### 5. SUBSEQUENT GROWTH

The runaway radius, which is derived in §4.2 as a function of turbulence strength, is the typical radius of planetesimals in the oligarchic growth of planetary embryos subsequent to runaway growth. Thus, the runaway radius has a strong effect on the growth of embryos, or the formation of planets. Kobayashi et al. (2011) conducted simulations for the formation and growth of planetary embryos through collisional merge and fragmentation, taking into account enhancement of the collisional cross section by a thin atmosphere, which is mainly important for Mars-sized or larger planetary embryos. Kobayashi et al. (2011) did not include turbulent stirring, but instead set the initial planetesimal radius as a parameter. Runaway growth occurs from the beginning in their simulations. Therefore, the initial planetesimal radii that were set almost correspond to the runaway radii obtained in the present work. For kilometer-sized or larger planetesimals, fragments caused by collisional shattering are re-accumulated by self-gravity, which determines the effective collisional strength of the planetes-



imals. Small planetesimals are effectively brittle due to low self-gravity. The growth of planetary embryos via collisions with small initial planetesimals easily stalls due to a reduction of the planetesimals caused by active collisional fragmentation and the rapid radial drift of the yielded fragments. The resultant embryos depend on the typical planetesimal size during oligarchic growth of the embryos; If small planetesimals start runaway growth, planetary embryos grow via collisions with small planetesimals and the collisional fragmentation of the small planetesimals is too effective to form massive embryos. On the other hand, larger representative planetesimals at the onset of runaway growth require a longer timescale for the formation of embryos. Therefore, we expect that strong turbulence results in large runaway radii and produces massive planetary embryos, whereas small runaway radii caused by weak turbulence is required for the rapid formation of planets.

When the probable planetesimal sizes for the masses and formation timescales of planets are determined, constraints can then be conversely given on the strength of turbulence. The turbulence strength  $f_{d,\text{run}}$  required for the runaway radius  $r_{p,\text{run}}$  is obtained from Eq. (29) or (30). Under the assumption of the power-law disk of Eqs. (5) and (6),  $f_{d,\text{run}}$  is given by the larger of  $f_{d,\text{run},c}$  or  $f_{d,\text{run},g}$ , where

$$f_{d,\text{run},c} = 9.7 \times 10^{-4} \frac{f_{\text{ice}} x_s}{x_g^2} \left( \frac{r_p}{100 \text{ km}} \right) \left( \frac{a}{5.2 \text{ AU}} \right)^{-3/2} \times \left( \frac{M_*}{M_\odot} \right), \quad (31)$$

$$f_{d,\text{run},g} = 6.7 \times 10^{-9} x_g \left( \frac{r_p}{100 \text{ km}} \right)^2 \left( \frac{H}{0.37 \text{ AU}} \right)^{-1} \times \left( \frac{\rho_s}{0.1 \text{ g/cm}^3} \right)^{1/2} \left( \frac{M_*}{M_\odot} \right)^{1/2}, \quad (32)$$

are derived from Eqs. (29) and (30), respectively. Because the collisional effect is more important than damping by gas drag,  $f_{d,\text{run}}$  is determined by  $f_{d,\text{run},c}$ . Constraints on  $f_d$  are given by calculating  $f_{d,\text{run}}$  below.

For the formation of Jupiter, a core should grow up to approximately 10 Earth masses within the disk lifetime and induce rapid gas accretion (Ikoma et al. 2000). The lifetimes of disks are inferred from the thermal emission of dust as  $\sim 1\text{--}6$  Myr (Briceño et al. 2001; Haisch et al. 2001; Najita & Kenyon 2014). In the simulation by Kobayashi et al. (2011), a  $10M_\oplus$  core can be formed from 100 km radius planetesimals at 5 AU in the 10 MMSN disk within 1 Myr<sup>6</sup>. From Eqs. (31) and (32),  $f_{d,\text{run}} \sim 10^{-4}$  is required for  $r_{p,\text{run}} \sim 100$  km at 5 AU in 10 MMSN. Fig. 4 shows  $f_d$  (or  $\alpha$  for  $H_{\text{res},0} \approx H$ ), which can prepare the conditions for the formation of Jupiter given by  $r_{p,\text{run}} = 30\text{--}300$  km at 5–6 AU in disks with  $x_g = x_s = 10$ .

<sup>6</sup> In their result for 100 km radius initial planetesimals in the 10 MMSN (Fig. 5 of Kobayashi et al. (2011)), cores are larger than  $10M_\oplus$  inside 10 AU at 10 Myr. The core formation timescale at 5 AU is approximately 10 times shorter than that at 10 AU; therefore, a  $10M_\oplus$  core at 5 AU can be formed within 1 Myr. The data of the simulation conducted by Kobayashi et al. (2011) do show the formation of  $10M_\oplus$  cores within 1 Myr.

Saturn’s core forms in the disk after the formation of Jupiter. The gap opening by Jupiter assists the rapid growth of Saturn’s core at the outer edge of the gap, where the radial drift due to gas drag is negligible. The collisional fragments produced during core formation accelerate the growth of the core, and the supply of fragments produced in the outer disk induces further rapid growth. These effects allow the rapid formation of Saturn’s core within  $\sim 10^6$  years after gap opening by Jupiter, and the rapid formation may explain the massive core of Saturn (Kobayashi et al. 2012). For the rapid growth of Saturn’s core in 10 MMSN, 100 km radius or smaller planetesimals are required, which is satisfied for  $f_d \lesssim 3 \times 10^{-4}$  ( $\alpha \lesssim 8 \times 10^{-3}$  for  $H_{\text{res},0} = H$ ) in the 10 MMSN disk (see Fig. 6). This upper limit is similar to the condition for Jupiter. If Jupiter can be formed via other mechanisms in the MMSN disk, then kilometer sized or smaller planetesimals are required for the rapid formation of Saturn’s core, which corresponds to  $\alpha \lesssim 10^{-3}$  for  $H_{\text{res},0} = H$ .

On the other hand, the formation age of Mars estimated from the amount of W isotope in the mantle is 2–4 Myr (Dauphas & Pourmand 2011). For 10 MMSN (MMSN), the early formation of Mars may be explained by planetesimals with radii of  $\lesssim 10$  km (5–30 km) (Kobayashi & Dauphas 2013). The disk inside the snow line ( $a < 2.7$  AU) has  $f_{\text{ice}} \approx 0.24$  (Hayashi 1981). From Eqs. (31) and (32), the formation of Mars requires  $f_d < 2 \times 10^{-5}$  at 1 AU ( $f_d < 1 \times 10^{-5}$  at 1.5 AU) in the 10 MMSN disk, while  $f_d \approx 10^{-4} - 10^{-3}$  is suitable at 1–1.5 AU in the MMSN (see Fig. 6).

In addition, main-belt asteroids with radii smaller than 50–100 km have a  $d \ln n_s / d \ln m$  slope of  $\sim -11/6$ , which is similar to the outcome of collisional cascade (Bottke et al. 2005), while larger main-belt asteroids except for the largest bodies (Ceres, Vesta, and Pallas) have shallower slopes. The main-belt asteroids, except for the largest asteroids, have a peak of  $m^2 n_s$  in the radius range of 50–100 km. The onset of runaway growth causes a similar shaped peak around the runaway radius (see Figs. 1 and 5). Assuming that the radius of 50–100 km in the main belt corresponds to the planetesimal radius,  $f_d = (5 \dots 9) \times 10^{-5}$  at 2 AU ( $f_d = (1 \dots 3) \times 10^{-5}$  at 3 AU) in the 10 MMSN and  $f_d = (4 \dots 10) \times 10^{-4}$  at 2 AU ( $f_d = (1 \dots 3) \times 10^{-3}$  at 3 AU) in the MMSN.

In Fig. 6, the constraints on the turbulence strength ( $f_d$  or  $\alpha$ ) are summarized based on these considerations. Jupiter cannot be formed via planetesimal accretion in the MMSN; therefore, there is no hatched region for Jupiter in the MMSN. If the Solar System was formed in a disk as massive as the 10 MMSN disk, then the radial distribution of turbulence is that shown in the bottom panel of Fig. 6. In the inner disk where terrestrial planets formed, turbulence is expected to have been weak, and thus the disk may be a “dead zone” where MRI is substantially suppressed. On the other hand, the disk beyond 2 AU is expected to have had relatively high  $f_d$  or  $\alpha$ . Note that the radial dependence of  $f_d$  or  $\alpha$  also depends on that of  $\Sigma_g$  and  $\Sigma_s$ . If the surface density for solid and gas is comparable to that of 10 MMSN around 5 AU, as required for the formation of Jupiter’s core, then  $\alpha$  required for the formation of Mars in the disk with  $\Sigma_g \propto \Sigma_s \propto a^{-1}$  is approximately 3 times larger than



that estimated in Fig. 6.

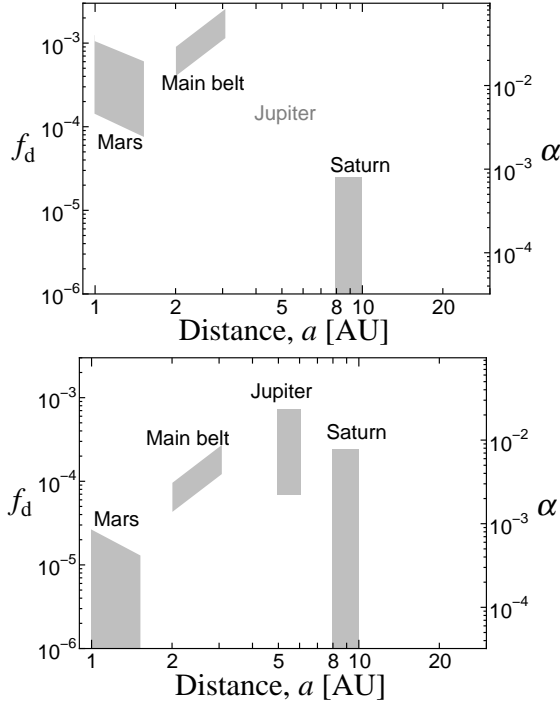


FIG. 6.— Turbulence strength  $f_d$  or  $\alpha$ , required for the formation of Mars, Jupiter, and Saturn for the MMSN (top panel) and 10 MMSN (bottom panel). The formation of the  $\sim 10M_\oplus$  core required for Jupiter via core accretion is difficult to accomplish with the MMSN. The value of  $\alpha$  is estimated under the assumption of  $H_{\text{res},0} = H$ .

In MRI,  $\alpha$  is a dimensionless coefficient that is proportional to the turbulent accretion stress integrated over the elevation of a disk. The saturation value of  $\alpha$  in MRI simulations depends on conditions such as the initial vertical net magnetic field  $\langle B_{z,0} \rangle$ , and the ohmic resistivity  $\eta$ . Based on MRI simulations, Okuzumi & Hirose (2011) empirically derived

$$\alpha = \frac{510}{\beta_{z,0}} \exp\left(\frac{0.54H_{\text{res},0}}{H}\right) + 0.0011 \exp\left(\frac{3.6H_{\Lambda,0}}{H}\right), \quad (33)$$

where  $\beta_{z,0} = 8\pi\rho_{\text{gas}}\langle B_{z,0} \rangle$  is the plasma beta and  $H_{\Lambda,0}$  is the vertical width of the dead zone that includes the resistive MRI zone. The charge reaction network gives the scale heights of the dead zones,  $H_{\text{res},0}$  and  $H_{\Lambda,0}$ . However, the results depend on the total surface area of solid particles (e.g., Ilgner & Nelson 2006). In addition,  $\alpha$  depends on  $\langle B_{z,0} \rangle$ , which are determined by the radial transport of large-scale magnetic fields in accretion disks (Takeuchi & Okuzumi 2014). Therefore, the  $\alpha$  value is uncertain due to conditions such as the magnetic fields and the total surface area of particles. However, the results from attempts at simulation in this work may provide some constraints on these physical conditions during planet formation.

## 6. SUMMARY AND DISCUSSION

Turbulent stirring increases the relative velocities between planetesimals and thus delays the onset of runaway growth; instead orderly growth occurs, in which

the solid surface density or the total mass of planetesimals is mainly determined by planetesimals with the weighted average radius. The relative velocity between the representative planetesimals,  $v_r$ , is much higher than their surface escape velocity,  $v_{\text{esc}}$ , in the early stage. The representative planetesimals get larger due to collisional growth, so that the Safronov parameter  $\Theta = (v_r/v_{\text{esc}})^2$  is smaller and the runaway growth of planetesimals then starts when  $\Theta \sim 1$ . This has been confirmed via simulations described in Section 3. In addition, we have analytically derived the following solutions, which perfectly reproduce the results of the simulations.

1. When the representative planetesimals are small or the solid surface density is large, the random velocity is determined by the collisional effects (damping and coagulation of planetesimals) and turbulent stirring, which is given by Eq. (25).
2. For large planetesimals and/or low solid surface density, the random velocity is given by the equilibrium between gas damping and turbulent stirring, as given by Eq. (28).
3. When  $\Theta \approx 2.25$  or  $v_r \approx 1.5v_{\text{esc}}$ , the runaway growth of bodies begins. Using the random velocities given in Eqs. (25) and (28), the radius of planetesimals at the onset of runaway growth,  $r_{\text{p,run}}$ , is determined by the smaller of Eqs. (29) or (30). For the internal density  $\rho_s = 0.1 \text{ g/cm}^3$  ( $1 \text{ g/cm}^3$ ), if  $r_{\text{p,run}} \lesssim 400 \text{ km}$  ( $200 \text{ km}$ ), then the collisional effect is more important than the gas drag, and thus  $r_{\text{p,run}}$  is given by Eq. (29).

Subsequent growth is strongly affected by the radius of planetesimals at the onset of runaway growth  $r_{\text{p,run}}$  because their typical size is almost unchanged during subsequent growth. Taking into account the previous studies on planet formation starting from initially large planetesimals in non-turbulent disks, the following has been determined:

1. For the formation of Jupiter via the core accretion scenario,  $\sim 10M_\oplus$  is formed within the disk lifetime, which requires  $\sim 30\text{--}300 \text{ km}$  planetesimals in a massive disk  $x_g \sim x_s \sim 10$  (Kobayashi et al. 2011). The turbulence strength with  $f_d \sim 10^{-3}\text{--}10^{-4}$  ( $\alpha \sim 3\text{--}30 \times 10^{-3}$  for  $H_{\text{res},0} = H$ ) results in  $r_{\text{p,run}} \sim 30\text{--}300 \text{ km}$  at 5–6 AU in the 10 MMSN disk, which may produce a massive core for the formation of Jupiter.
2. For the formation of Saturn, the gap opening by Jupiter assists the rapid accretion of Saturn's core after the formation of Jupiter; if representative planetesimals at the onset of runaway growth are smaller than 100 km, then Saturn's core can be formed within  $10^6$  years after the formation of Jupiter (Kobayashi et al. 2012). Therefore, the formation of Saturn requires a turbulence strength  $f_d \lesssim 2 \times 10^{-4}$  ( $\alpha \lesssim 10^{-2}$  for  $H_{\text{res},0} = H$ ), which satisfies the conditions for the formation of Jupiter.
3. The core formation timescale of Mars is estimated to be 2–4 Myrs (Dauphas & Pourmand 2011),

which requires 10 km or smaller planetesimals at the onset of runaway growth in a massive disk required to form Jupiter's core. In the 10 MMSN disk, weaker turbulence with  $f_d \lesssim 10^{-5}$  ( $\alpha \lesssim 3 \times 10^{-4}$  for  $H_{\text{res},0} = H$ ) results in  $r_{\text{p,run}} \lesssim 10$  km around 1 AU, which may form Mars rapidly. The condition for the formation of Mars corresponds to  $f_d \lesssim 10^{-5}$  ( $\alpha \lesssim 3 \times 10^{-4}$  for  $H_{\text{res},0} = H$ ) in the 10 MMSN disk.

4. The proposed fossil feature in the size distribution of main-belt asteroids has a radius of approximately 50–100 km, which is explained by turbulence with  $f_d \sim 10^{-4}$  ( $\alpha \sim 10^{-2}$  for  $H_{\text{res},0} = H$ ) for the 10 MMSN disk.
5. The turbulent strength expected for formation of the Solar System is summarized in Fig. 6, assuming the Solar System was formed in the 10 MMSN disk. The inner disk where terrestrial planets formed may have low  $\alpha$ , while  $\alpha$  is larger in the outer disk.

Kobayashi & Löhne (2014) investigated the formation of the debris disk caused by planet formation in planetesimal disks. Planetary embryos formed from planetesimals induce collisional fragmentation of remnant planetesimals, which can form debris disks after gas depletion. Narrow disks with 100 km planetesimals around 30 AU

can explain the evolutionary trend of infrared excesses of debris disks observed at 18 and 70  $\mu\text{m}$  by the Spitzer Space Telescope. The turbulent strength required for debris disks is similar to that for the outer solar system.

The formation of Jupiter required a massive disk. However, the surface density of planetesimals constructed via the collisional evolution of bodies is different from the initial solid surface density (Okuzumi et al. 2012). In addition, pebbles grow in the outer disk and drift to the inner disk. The collisional cross sections between pebbles and planetary embryos are high (e.g., Ormel & Klahr 2010). The growth of embryos may be accelerated due to the accretion of pebbles that drift from the outer disk (Bromley & Kenyon 2011; Lambrechts & Johansen 2014; Levison et al. 2015). Therefore, if the initial protoplanetary disk is even less massive than 10 MMSN, then the formation of Jupiter may be possible. In future work, we should address continuous collisional growth from dust to planets in turbulent disks, which may reveal the formation of the debris disk as well as planet formation.

We thank Neal Turner for his valuable comments on our manuscript. This work was supported by Grants-in-Aid for Scientific Research (Nos. 26287101, 23103005, 23103004, 15H02065) from the Ministry of Education, Culture, Sports, Science and Technology (MEXT) of Japan and by the Astrobiology Center Project of the National Institute of Natural Sciences (NINS) (Grant Number AB271020).

## REFERENCES

- Adachi, I., Hayashi, C., & Nakazawa, K. 1976, *Progress of Theoretical Physics*, 56, 1756
- Balbus, S. A., & Hawley, J. F. 1991, *ApJ*, 376, 214
- Bottke, W. F., Durda, D. D., Nesvorný, D., et al. 2005, *Icarus*, 175, 111
- Briceño, C., Vivas, A. K., Calvet, N., et al. 2001, *Science*, 291, 93
- Bromley, B. C., & Kenyon, S. J. 2011, *ApJ*, 731, 101
- Dauphas, N., & Pourmand, A. 2011, *Nature*, 473, 489
- Gressel, O., Nelson, R. P., & Turner, N. J. 2012, *MNRAS*, 422, 1140
- Haisch, K. E., Jr., Lada, E. A., & Lada, C. J. 2001, *ApJ*, 553, L153
- Han, W., Yu, J., & Wang, Q. 2000, *Journal of Applied Physics*, 88, 4404
- Hayashi, C. 1981, *Progress of Theoretical Physics Supplement*, 70, 35
- Hori, Y., & Ikoma, M. 2010, *ApJ*, 714, 1343
- Ida, S., Guillot, T., & Morbidelli, A. 2008, *ApJ*, 686, 1292
- Ikoma, M., Nakazawa, K., & Emori, H. 2000, *ApJ*, 537, 1013
- Inaba, S., Tanaka, H., Nakazawa, K., Wetherill, G. W., & Kokubo, E. 2001, *Icarus*, 149, 235
- Ilgner, M., & Nelson, R. P. 2006, *A&A*, 445, 205
- Johansen, A., Blum, J., Tanaka, H., et al. 2014, *Protostars and Planets VI*, 547
- Johnson, K.L., Kendal, K., Roberts, A.D. 1971, *Proc. R. Soc. Lond. A*, 324, 301
- Kataoka, A., Tanaka, H., Okuzumi, S., & Wada, K. 2013, *A&A*, 554, A4
- Kataoka, A., Tanaka, H., Okuzumi, S., & Wada, K. 2013, *A&A*, 557, L4
- Kimura, H., Wada, K., Senshu, H., & Kobayashi, H. 2015, *ApJin press*.
- Kobayashi, H. 2015, *Earth, Planets and Space* 67, 60
- Kobayashi, H., & Dauphas, N. 2013, *Icarus*, 225, 122
- Kobayashi, H., Löhne, T. 2014, *MNRAS*, 442, 3266
- Kobayashi, H., Ormel, C. W., & Ida, S. 2012, *ApJ*, 756, 70
- Kobayashi, H., & Tanaka, H. 2010, *Icarus*, 206, 735
- Kobayashi, H., Tanaka, H., Krivov, A. V., & Inaba, S. 2010, *Icarus*, 209, 836
- Kobayashi, H., Tanaka, H., & Krivov, A. V. 2011, *ApJ*, 738, 35
- Kokubo, E., Ida, S. 1996, *Icarus* 123, 180
- Kokubo, E., & Ida, S. 1998, *Icarus*, 131, 171
- Lambrechts, M., & Johansen, A. 2014, *A&A*, 572, A107
- Levison, H. F., Kretke, K. A., & Duncan, M. J. 2015, *Nature*, 524, 322
- Mizuno, H. 1980, *Progress of Theoretical Physics*, 64, 544
- Najita, J. R., & Kenyon, S. J. 2014, *MNRAS*, 445, 3315
- Ohtsuki, K. 1992, *Icarus*, 98, 20
- Ohtsuki, K., Stewart, G. R., & Ida, S. 2002, *Icarus*, 155, 436
- Okuzumi, S., & Hirose, S. 2011, *ApJ*, 742, 65
- Okuzumi, S., Tanaka, H., Kobayashi, H., & Wada, K. 2012 *ApJ*, 752, 106
- Okuzumi, S., & Ormel, C. W. 2013, *ApJ*, 771, 43
- Ormel, C. W., & Okuzumi, S. 2013, *ApJ*, 771, 44
- Ormel, C. W., Dullemond, C. P., & Spaans, M. 2010b, *Icarus*, 210, 507
- Ormel, C. W., & Klahr, H. H. 2010, *A&A*, 520, A43
- Roder, A., Kob, W., & Binder, K. 2001, *J. Chem. Phys.*, 114, 7602
- Shchipalov, Y. K. 2000, *Glass and Ceramics*, 57, 374
- Suyama, T., Wada, K., Tanaka, H., & Okuzumi, S. 2012, *ApJ*, 753, 115
- Suyama, T., Wada, K., & Tanaka, H. 2008, *ApJ*, 684, 1310
- Suzuki, T. K., Muto, T., & Inutsuka, S.-i. 2010, *ApJ*, 718, 1289
- Takeuchi, T., & Okuzumi, S. 2014, *ApJ*, 797, 132
- Tromans, D. & Meech, J. A. *Minerals Engineering*, 14, 1359
- Völk, H. J., Jones, F. C., Morfill, G. E., & Röser, S. 1980, *A&A*, 85, 316
- Wada, K., Tanaka, H., Okuzumi, S., et al. 2013, *A&A*, 559, A62
- Wada, K., Tanaka, H., Suyama, T., Kimura, H., & Yamamoto, T. 2009, *ApJ*, 702, 1490
- Weidenschilling, S. J. 1977, *MNRAS*, 180, 57
- Weidenschilling, S. J., Spaute, D., Davis, D. R., Marzari, F., Ohtsuki, K. 1997, *Icarus*, 128, 429
- Wetherill, G. W., Stewart, G. R. 1989, *Icarus* 77, 330
- Wiederhorn, S. M., & Johnson, H. 1971, *Journal of Applied Physics*, 42, 681
- Yang, C.-C., Mac Low, M.-M., & Menou, K. 2012, *ApJ*, 748, 79

Youdin, A. N., & Lithwick, Y. 2007, *Icarus*, 192, 588